


# Membrane Nanopores Induced by Nanotoroids via an Insertion and Pore-Forming Pathway

Fangsheng Wu,<sup>†</sup> Xiao Jin,<sup>†</sup> Zhou Guan, Jiaping Lin,<sup>\*</sup> Chunhua Cai,<sup>\*</sup> Liquan Wang, Yongsheng Li, Shaoliang Lin, Pengfei Xu, and Liang Gao

 Cite This: *Nano Lett.* 2021, 21, 8545–8553

 Read Online

ACCESS |

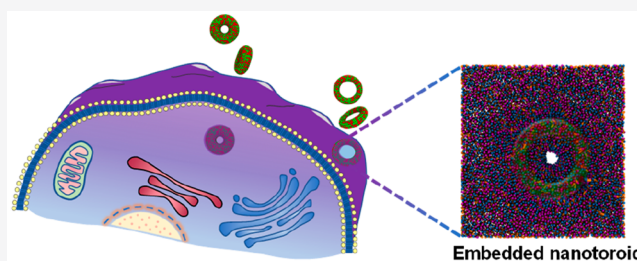
 Metrics & More

 Article Recommendations

 Supporting Information

**ABSTRACT:** The formation of membrane nanopores is one of the crucial activities of cells and has attracted considerable attention. However, the understanding of their types and mechanisms is still limited. Herein, we report a novel nanopore formation phenomenon achieved through the insertion of polymeric nanotoroids into the cellular membrane. As revealed by theoretical simulations, the nanotoroid can embed in the membrane, leaving a nanopore on the cell. The through-the-cavity wrapping of lipids is critical for the retention of the nanotoroid in the membrane, which is attributed to both a relatively large inner cavity of the nanotoroid and a moderate attraction between the nanotoroid and membrane lipids. Under the guidance of the simulation predictions, experiments using polypeptide toroids as pore-forming agents were performed, confirming the unique biophysical phenomenon. This work demonstrates a distinctive pore-forming pathway, deepens the understanding of the membrane nanopore phenomenon, and assists in the design of advanced pore-forming materials.

**KEYWORDS:** Membrane nanopores, Pore-forming pathway, Nanotoroid, CGMD simulations



Cellular material transport between cells and surroundings is critical for regulating life activities, decoding cell function, and controlling cell fate and identity.<sup>1–4</sup> Penetration and endocytosis are common routes for material transport. In addition, membrane nanopores formed by proteins act as transport channels between cells and the external matrix for diverse cargoes.<sup>5–8</sup> In particular, sub-micrometer materials can be delivered into cells more rapidly through membrane nanopores than through other uptake pathways.<sup>9</sup> Membrane nanopores are crucial in cellular lifetimes.

According to the features of nanopore formation, cellular pore-forming behaviors can be divided into two categories: biochemical and physical.<sup>5,9</sup> In biochemical nanopore formation, special biochemical materials, typically pore-forming proteins (PFPs), embed on the membrane bilayer via biochemical interactions and further assemble into toroids to form cellular nanopores.<sup>10–14</sup> Depending on the types of the PFPs, the diameter of the formed membrane pores varies from several nanometers (e.g., 1 nm for aerolysin and 3 nm for lysenin) to tens of nanometers (e.g., 25 nm for pneumolysin and 25–30 nm for cholesterol-dependent cytolysins).<sup>14–16</sup> Some amphiphilic peptides and surfactants can also form nanopores on the cellular membrane in a similar embedding–assembling manner.<sup>17</sup> Additionally, nanopores can be generated by the uptake of some nanostructures in the cellular membrane. For example, when carbon nanotubes are taken up in the membrane, their tubular structures act as trans-

membrane channels.<sup>18,19</sup> In contrast, in the physical category, nanopores are generated by physical mechanisms, such as electroporation, thermal treatments, and nanoneedles.<sup>20,21</sup> In physical nanopore formation, nanopores are generated by remodeling the membrane bilayer and forming transient discontinuities on the cell membrane.<sup>5</sup> For example, nanoneedles are capable of squeezing the membrane bilayer under external force to create nanopores in the cellular membrane.<sup>22</sup>

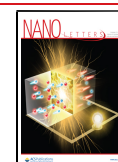
However, the mechanism behind pore-forming behaviors is not yet well-known. There is a lack of fundamental understanding of this important cellular activity. In addition to those mentioned above, it is not clear whether other nanopore-forming mechanisms exist. Further investigations are needed to obtain deep insights into the formation of nanopores on the cellular membrane.

Herein, combining theoretical simulations and experimental studies, we report a novel pore-forming phenomenon in cells that is generated by the insertion of nanotoroids into the cellular membrane. Coarse-grained molecular dynamics (CGMD) simulations revealed that nanotoroids with a

**Received:** April 2, 2021

**Revised:** September 1, 2021

**Published:** October 8, 2021



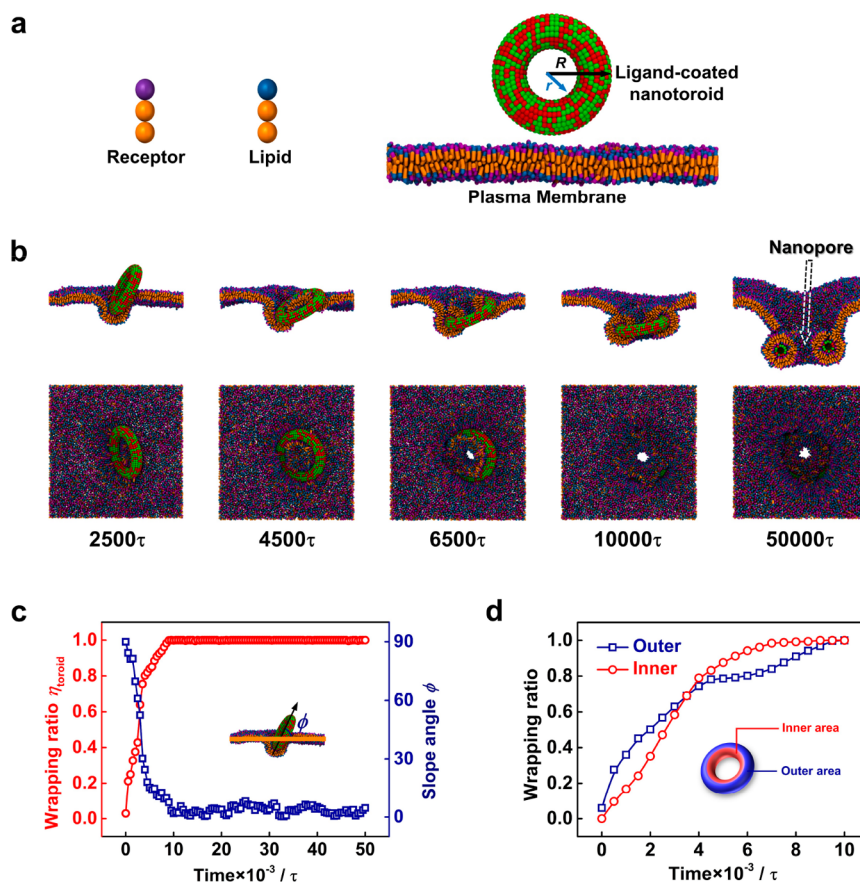


**Figure 1.** Simulations of the insertion and pore-forming behavior of nanotoroids on the membrane. (a) Coarse-grained models used in the simulations. The plasma membrane was constructed by receptors and lipids. The nanotoroid was constructed by surface beads (green) with ligands (red). Black and blue arrows show  $R$  and  $r$ , respectively. (b) Representative snapshots of the pore-forming behavior of a nanotoroid ( $\rho = 1.5$ ,  $\epsilon_{\text{int}} = 4k_{\text{b}}T$ ). To show the structure of the membrane nanopore clearly, the nanotoroid was cut across in the final snapshot. (c) Wrapping ratio of the nanotoroid  $\eta_{\text{toroid}}$  and the slope angle between the nanotoroid and membrane plane  $\phi$ . (d) Wrapping ratio of the inner and outer areas of the nanotoroid. An illustration of the inner and outer areas of the nanotoroid surface is shown in the inset.

relatively large inner cavity and moderate attraction with cellular lipids were preferentially retained in the cellular membrane, creating a nanopore. This unique pore-forming behavior was further confirmed by experimental observations using polypeptide toroids as pore-forming agents.

## RESULTS AND DISCUSSION

**Pore-Forming Behavior of Nanotoroids on the Cellular Membrane.** In this work, coarse-grained molecular dynamics (CGMD) simulations were performed.<sup>23–29</sup> A simulation system containing a ligand-decorated nanotoroid and a plasma membrane was constructed. The models are illustrated in Figure 1a. The nanotoroid was constructed from randomly distributed coarse-grained beads. Half of the beads were hydrophobic beads, and the other half were set as ligands. The size of the nanotoroid was characterized by the radius of the nanotoroid,  $R$  (fixed at  $12\sigma$  in simulations;  $\sigma$  is the length unit in the simulations), and the radius of the nanotoroid cavity,  $r$  (varied from  $2\sigma$  to  $8\sigma$  in simulations). The aspect ratio of the nanotoroid is defined as  $\rho = R/r$ , where a larger  $\rho$  value means a smaller cavity. Three kinds of nanotoroids ( $\rho = 6, 2, 1.5$ ) were examined in the simulations. The plasma membrane was composed of phospholipids. As illustrated in Figure 1a, the lipids were coarse-grained, consisting of three beads connected by harmonic bonds. The one head bead was hydrophilic, and

the two tail beads were hydrophobic.<sup>30–33</sup> Half of the lipids were receptors that can bind to the ligands. The strength of attraction between the membrane receptor and nanotoroid ligand ( $\epsilon_{\text{int}}$ ) was  $2–5 k_{\text{b}}T$ , which is an appropriate range for ligand–receptor interaction.<sup>34</sup> Detailed information regarding the models can be found in Sections 1.1 and 1.2 of the Supporting Information.

The cellular uptake of these nanotoroids under various conditions was then studied. Interestingly, we found that stable membrane nanopores could be generated by a nanotoroid with  $\rho = 1.5$  under  $\epsilon_{\text{int}} = 4.0 k_{\text{b}}T$ . Since stable nanopores are formed on the cellular membrane, such a phenomenon could be classified as cellular pore formation. The results are presented in Figure 1b, which depicts a top view and a side view of the pore-forming behavior. Videos of the pore-forming behavior of the nanotoroid are provided in the Supporting Information. After the initial contact, the nanotoroid exhibited a “lying-down” entry posture and was gradually wrapped by the lipids. Meanwhile, the membrane became curved. Due to the interaction between the membrane receptors and the ligands located within the nanotoroid cavity, the lipids were driven to cover the nanotoroid cavity. Both the outer surface and the inner cavity of the nanotoroid were finally wrapped by the lipids. To gain insights into the pore-forming process, we defined the evolutionary wrapping ratio of the nanotoroid,

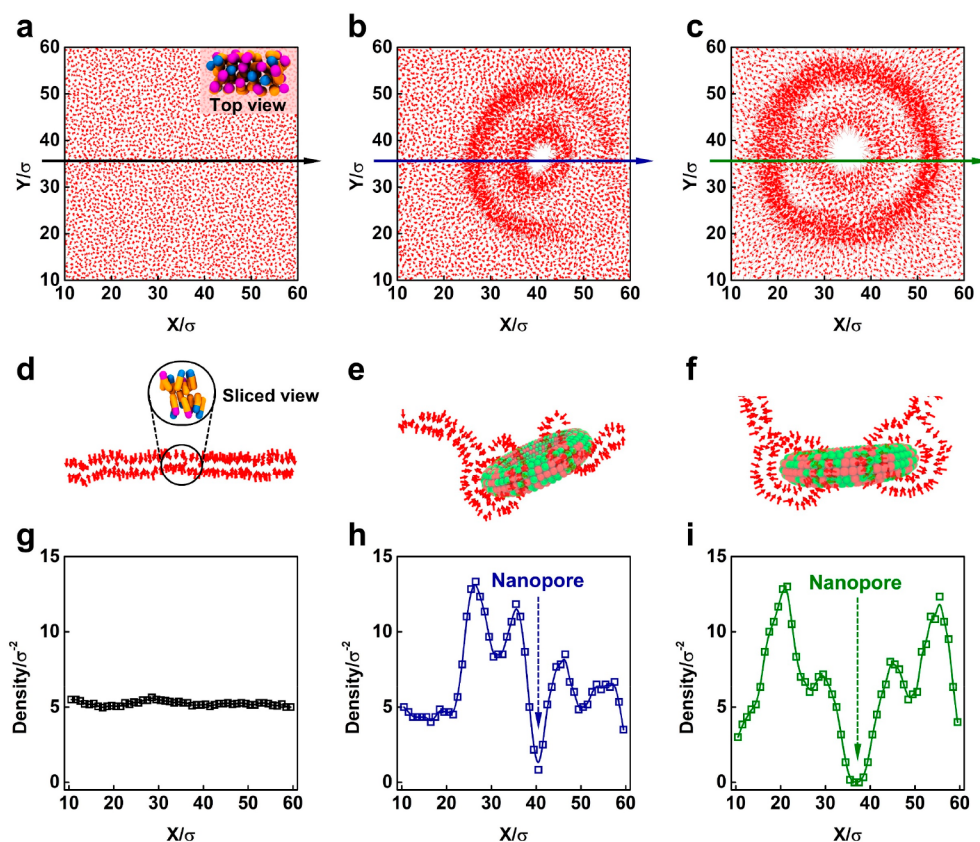


**Figure 2.** Variation in membrane disruption induced by the insertion of nanotoroids. (a–c) Distribution variation of the head-to-tail vectors of lipids in the pore formation process. The times are (a)  $0\tau$ , (b)  $6500\tau$ , and (c)  $50000\tau$ . (d–f) Sliced view of the lipid areas along the arrow directions in (a–c). (g–i) Density profiles of lipid particles along the colored arrows in (a–c).

$\eta_{\text{toroid}}$  (denoting engulfment by lipids), and the orientation angle between the nanotoroid and the membrane plane,  $\varphi$  (the definition of  $\varphi$  is shown in the inset of Figure 1c). Figure 1c shows the variation in  $\eta_{\text{toroid}}$  and  $\varphi$  with time. In the cellular uptake process,  $\eta_{\text{toroid}}$  increases while  $\varphi$  decreases. After  $\eta_{\text{toroid}}$  reaches 1.0 at  $(1 \times 10^4)\tau$ ,  $\varphi$  is stable at approximately  $5^\circ$ , indicating that the nanotoroid is almost parallel to the membrane plane. The nanotoroid stays in the membrane instead of being endocytosed. By careful examination, we found that the lipids wrapped through the cavity merged with the lipids outside the nanotoroid. The fusion of the two parts of the membrane resulted in the nanotoroid being localized stably in the membrane. The finding of nanotoroid-induced membrane nanopores indicates a biophysical phenomenon for cellular internalization: i.e., insertion of a nanotoroid in the cellular membrane. Such a phenomenon is based on a novel uptake behavior that is different from typical endocytosis behavior. In a typical endocytosis process, the nanoparticles are first wrapped by lipids and then the wrapped nanoparticles detach from cellular membrane into the cell,<sup>1,34</sup> while in the present system, the wrapped toroids stably retain on the cellular membrane, leaving nanopores.

To better understand this pore-forming process, we marked the inner and outer areas of the nanotoroid by bisecting its surface area and calculated the evolutionary wrapping ratio of both the inner ( $\eta_{\text{inner}}$ ) and outer areas ( $\eta_{\text{outer}}$ ). The results are presented in Figure 1d (see the inset for the definition of the inner and outer areas). At the beginning, due to the initial contact between the nanotoroid and the membrane,  $\eta_{\text{outer}}$  was

approximately 0.05 while  $\eta_{\text{inner}}$  was 0. As the wrapping continued, the nanotoroid gradually laid down on the membrane surface. At this time,  $\eta_{\text{outer}}$  was larger than  $\eta_{\text{inner}}$ . When the lipids began to wrap through the nanotoroid cavity,  $\eta_{\text{inner}}$  increased rapidly and then became greater than  $\eta_{\text{outer}}$ . Finally, both the inner and outer areas were engulfed completely. Due to this unique through-the-cavity wrapping mechanism, the nanotoroid is inserted into the membrane. Additionally, we examined the effect of the distribution manner of the ligands on cellular uptake (see Figure S7). Three types of distribution manners for the nanotoroids were studied: namely, outside, inside, and spaced. It was found that the inside and spaced types of nanotoroids can both exhibit pore-forming behavior, while the outside type of nanotoroid cannot be fully wrapped, indicating that the existence of ligands on the inner surface area of the nanotoroid is critical for lipids to pass through the cavity of the nanotoroid as well as for the formation of membrane nanopores.

Because the embedded nanotoroid causes interference with the cell membrane, membrane disruption by the pore formation of the nanotoroid was accordingly investigated. We examined the membrane disruption in terms of variation in lipid distribution and orientation. The head-to-tail vectors of lipids from the top view (Figure 2a–c) and the sliced view (Figure 2d–f) were used to characterize the distribution and orientation of the lipids. The planar bilayer structure was altered to encapsulate the nanotoroid. The bilayer membrane showed a shape change when the pore structure was formed. To gain insight into the distribution changes of the lipids, the



density profiles of lipid particles along the diameter of the toroid were plotted. As shown in Figure 2g–i, the density distribution changed due to the uptake of nanotoroids. Peaks represent the aggregation of lipids, while valleys represent the escape of lipids. This indicates that lipids accumulated on the nanotoroid surface and formed a channel within the nanotoroid cavity. More information about the membrane change in the pore-forming process can be found in Section 1.8 of the Supporting Information.

The effects of the receptor–ligand binding strength  $\epsilon_{\text{int}}$  and the nanotoroid aspect ratio  $\rho$  on the cellular uptake process were then examined (see Figures S2 and S3 for more information). To systematically elucidate the uptake pathways of nanotoroids, a two-dimensional diagram in the space of  $\epsilon_{\text{int}}$  and  $\rho$  was constructed on the basis of the obtained data. As shown in Figure 3a, three interaction pathways were identified:

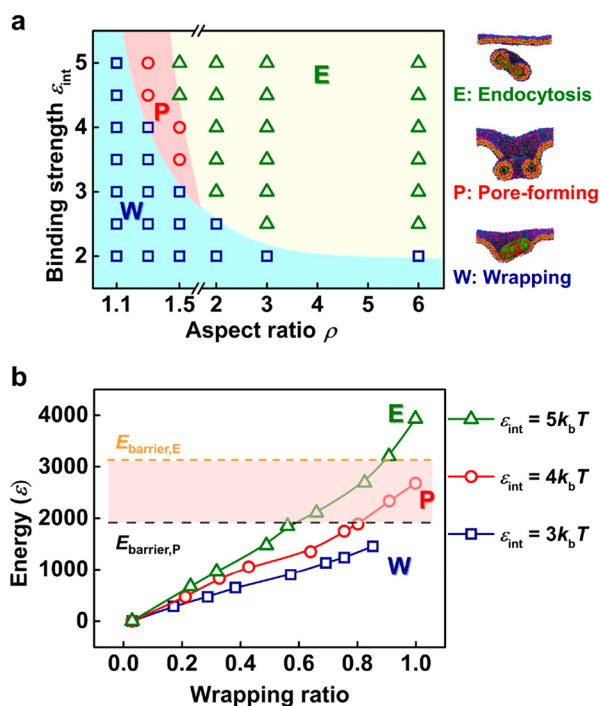


**Figure 3.** Effects of receptor–ligand binding strength and aspect ratio of nanotoroids on cellular uptake behavior. (a) Cellular uptake pathway diagram in the space of  $\rho$  and  $\epsilon_{\text{int}}$ . Regions corresponding to different pathways are shown in different colors. Abbreviations: E, endocytosis; W, wrapping; P, pore-forming. Typical snapshots of the three pathways are shown on the right of the figure. (b) Binding energy between the nanotoroid ( $\rho = 1.5$ ) and the membrane as a function of the wrapping ratio.  $E_{\text{barrier,P}}$  represents the energy barrier for pore formation.  $E_{\text{barrier,E}}$  represents the energy barrier for endocytosis. The colored area shows the pore-forming region.

namely, wrapping (denoted by W), endocytosis (denoted by E), and pore-forming (denoted by P). At lower  $\epsilon_{\text{int}}$  values (see the bottom region), the membrane–nanotoroid interaction is weak, giving rise to the wrapping pathway. At lower  $\rho$  values (see the left region), the nanotoroids cannot be fully wrapped. Larger values of  $\epsilon_{\text{int}}$  and  $\rho$  favor the endocytosis pathway (see the top and right regions). Nanotoroids with moderate  $\epsilon_{\text{int}}$  values and relatively large  $\rho$  values exhibit a pore-forming pathway. The pore-forming region is between the endocytosis region and the wrapping region (see Figures S4 and S5 for

more information), where  $\rho$  ranges from 1.3 to 1.5 and  $\epsilon_{\text{int}}$  varies from  $3.5k_bT$  to  $5.0k_bT$ . Detailed information can be found in Section 1.5 of the Supporting Information.

To deepen the understanding of the formation mechanism of membrane nanopores, the bending energy of the membrane ( $E_{\text{mem}}$ ) and the binding energy between the nanotoroid and the membrane ( $E_{\text{bind}}$ ) were calculated (see Section 1.9 of the Supporting Information for detailed information).<sup>35–38</sup> We take nanotoroids with  $\rho = 1.5$  as an example to examine the critical energy for pore-forming behavior. Due to possible membrane rupture, the nanotoroid must overcome the bending energy and the energy required for membrane rupture to translocate through the membrane. The bending energy for a fully wrapped nanotoroid can be considered the energy barrier for pore formation ( $E_{\text{barrier,P}}$ ). The value of  $\epsilon_{\text{int}}$  for pore formation was found to be marginally smaller than  $4.1k_bT$  (see Figure S10). Therefore,  $E_{\text{bind}}$  at  $\epsilon_{\text{int}} = 4.1k_bT$  can be considered the energy barrier for endocytosis ( $E_{\text{barrier,E}}$ ). As shown in Figure 3b, we consider the nanotoroid with  $\rho = 1.5$  and  $\epsilon_{\text{int}}$  values of  $3k_bT$ ,  $4k_bT$ , and  $5k_bT$ , which correspond to the three membrane–nanotoroid interaction pathways: wrapping, pore-forming, and endocytosis, respectively. For  $\epsilon_{\text{int}} = 3k_bT$ , the binding energy,  $E_{\text{bind}}$ , is smaller than  $E_{\text{barrier,P}}$ , so that only wrapping occurs. For the medium  $\epsilon_{\text{int}}$  value ( $\epsilon_{\text{int}} = 4k_bT$ ), the binding energy is larger than  $E_{\text{barrier,P}}$  but is insufficient to overcome the energy barrier for endocytosis,  $E_{\text{barrier,E}}$  (pore-forming behavior can be observed). When  $\epsilon_{\text{int}}$  increases to  $5k_bT$ , the  $E_{\text{bind}}$  value is large enough to overcome  $E_{\text{barrier,E}}$ , leading to complete endocytosis.

In addition, the energy changes as a function of the aspect ratio  $\rho$  were examined. As shown in Figures S11 and S12, a larger  $\rho$  value causes a larger  $E_{\text{bind}}$  value (the nanotoroid has more ligands due to a larger surface area) and a smaller  $E_{\text{mem}}$  value ( $E_{\text{mem}}$  is size-dependent). Moreover, nanotoroids with a large  $\rho$  value are not helpful for lipids to pass through the cavity due to space limitations. As a result of the interplay of these facts, nanopore formation is not favorable. With respect to a small  $\rho$  value, a nanotoroid with a large cavity is beneficial for lipid rearrangement to form a nanopore. These simulation results stress the point that membrane nanopores can be induced by adjusting the nanotoroid–membrane interaction and the aspect ratio of the nanotoroids.

**Experimental Observations of Nanopore Formation on the Cellular Membrane.** According to the simulation results, nanotoroids have the ability to create membrane nanopores. To experimentally verify the prediction, we prepared a set of aggregates, including toroids and spheres, by assembling poly( $\gamma$ -benzyl-L-glutamate) (PBLG)<sup>39–42</sup> and then examined their cell internalization into SMMC-7721 cells (detailed information on the preparation can be found in Sections 2.1 and 2.2 of the Supporting Information). Polypeptide aggregates usually have strong interactions with the cellular membrane due to both specific binding interactions (amino acids and polypeptides can act as ligands to bind membrane lipids) and nonspecific binding interactions (for example, hydrophobicity, roughness, and other surface characteristics can promote cellular contact and uptake).<sup>43,44</sup> The morphologies of these aggregates characterized by scanning electron microscopy (SEM) are presented in Figure 4a–d. The toroids with a small cavity ( $\rho = 6.1 \pm 0.6$ ) are denoted by toroid-1, the toroids with a moderate cavity ( $\rho = 4.1 \pm 0.3$ ) are denoted by toroid-2, and those with a large cavity ( $\rho = 1.8 \pm 0.1$ ) are denoted by toroid-3. Spherical

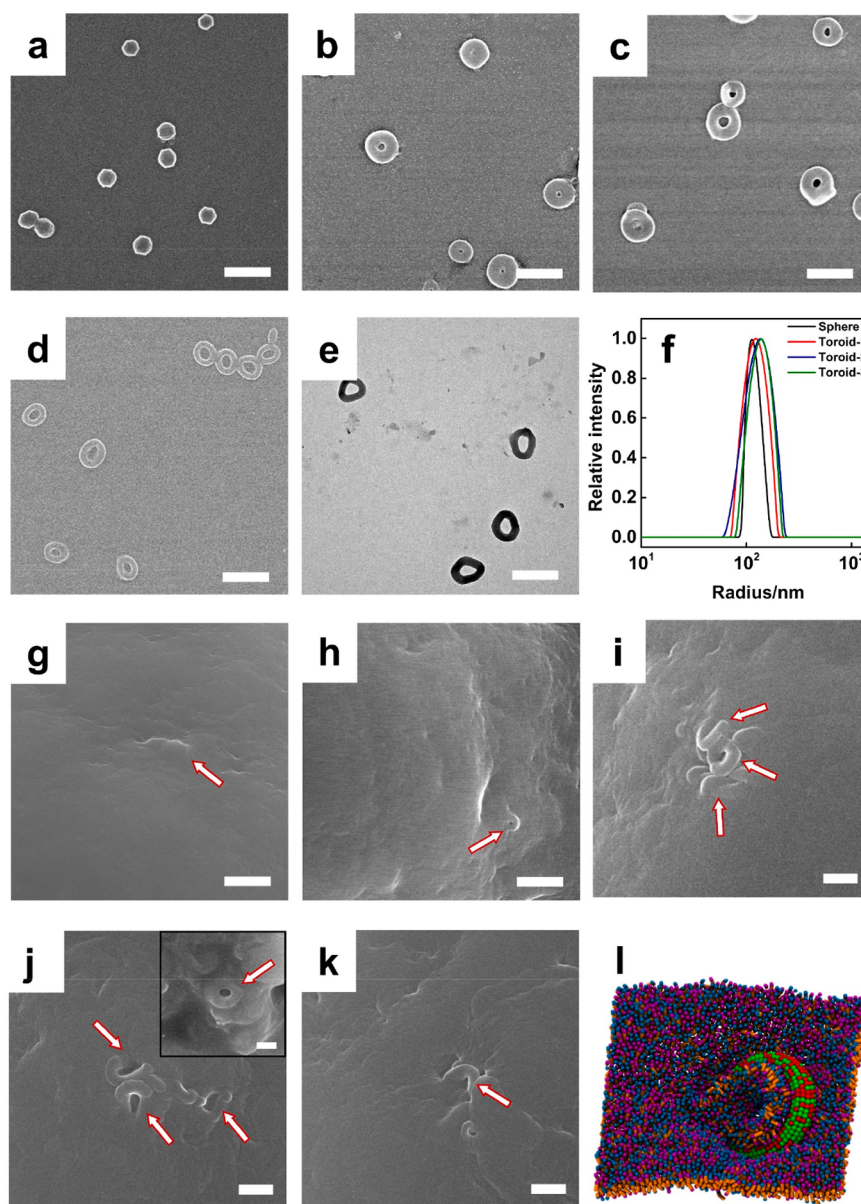


**Figure 4.** Experimental observations for the toroid-induced membrane nanopores. (a–d) SEM images of polypeptide spheres, toroid-1, toroid-2, and toroid-3, respectively. (e) TEM image of polypeptide toroid-3. (f) Hydrodynamic radii of polypeptide spheres, toroid-1, toroid-2, and toroid-3. (g–k) SEM images of cells incubated with polypeptide spheres (g), toroid-1 (h), toroid-2 (i), and toroid-3 (j, k). The red arrows indicate the position of the polypeptide aggregates. A cryo-SEM image is shown in the inset of Figure 4j. In (k), the membrane lipids across through the cavity of toroid-3 can be seen. (l) Pore-forming simulation snapshot at 6000 $\tau$ . Scale bars: 500 nm in (a–e), (g), and (h); 200 nm in (i–k) and inset of (j).

micelles were used as a comparison. The toroidal structures were also characterized by transmission electron microscopy (TEM). A representative image for toroid-3 is shown in Figure 4e. The hydrodynamic radius of these aggregates is shown in Figure 4f. The result indicates that all of these aggregates have a radius of approximately 130 nm. Details on the experimental information are available in sections 2.3 and 2.4 of the Supporting Information.

The internalization of aggregates usually causes changes in cell membrane morphology, which can be captured by SEM images.<sup>45–47</sup> Figure 4g–j shows the membrane surface of cells incubated with polypeptide aggregates. After 2 h of incubation, no membrane nanopores were observed for the sphere, toroid-1, and toroid-2 systems, which are consistent with the simulation predictions (for the details of the simulations, see

section 1.6 of the Supporting Information). However, membrane nanopores induced by toroid-3 can be clearly observed (see Figure S15 for more images). To eliminate the influence of drying on SEM sample preparation, a cryogenic scanning electron microscopy (cryo-SEM) observation was performed. The nanotoroid-induced membrane nanopore can also be captured by cryo-SEM (see the inset of Figure 4j). The size of the membrane pores reached hundreds of nanometers, which is consistent with the size of the toroid cavity. The membrane nanopores are identified by the appearance of a penetrating area in the cavity of the toroids. It should be noted that, as illustrated in Figure 4k, a part of the nanotoroid was covered by the membrane, and the whole nanotoroid could not be observed, showing the progress in the embedding of the nanotoroid into the membrane. This observation is quite

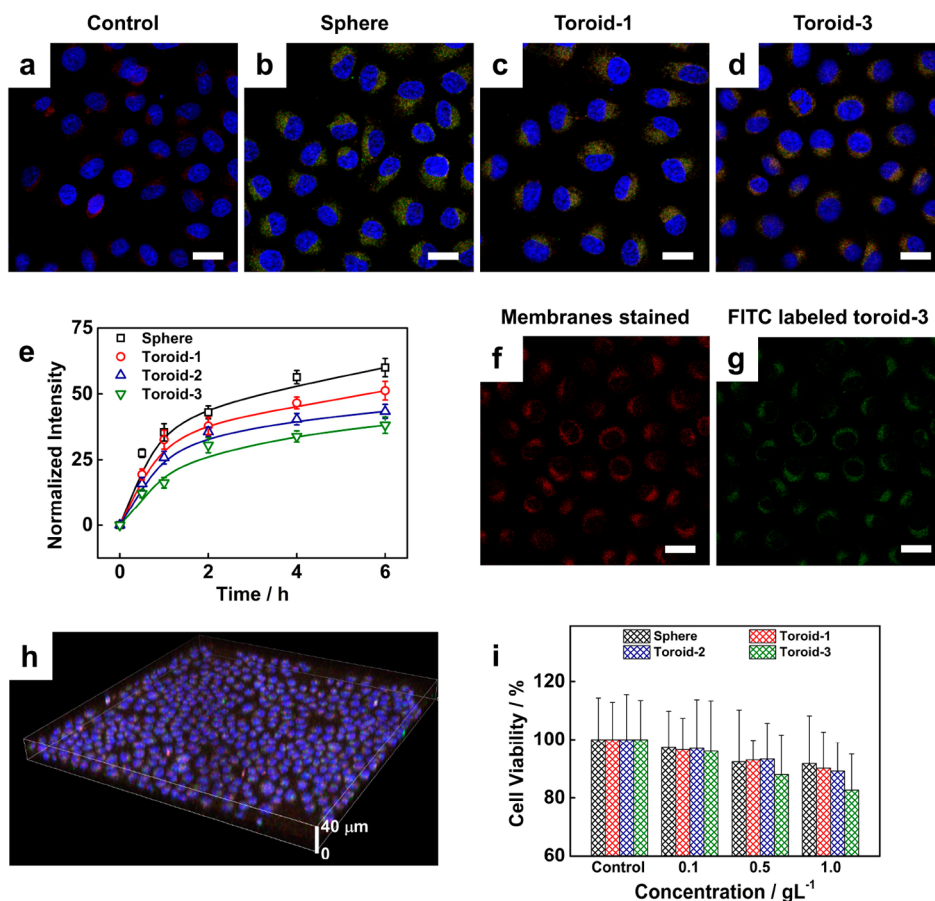


**Figure 5.** Cellular uptake behavior and cell cytotoxicity of polypeptide nanotoroids. (a–d) CLSM images of cells upon incubation with PBS, polypeptide spheres, toroid-1, and toroid-3. Confocal microscopy images portraying cell nuclei are shown in blue and polypeptide aggregates in green. (e) Profiles of the fluorescence intensity of spheres, toroid-1, toroid-2, and toroid-3 as a function of time, which were measured by flow cytometry and quantified from CLSM observations. (f, g) Confocal microscopy images portraying the cytoskeleton in red (f) and polypeptide toroid-3 in green (g). (h) 3D overlay image of cells after incubation with polypeptide toroid-3. (i) Cell viability after incubation with different polypeptide aggregates at various concentrations for 6 h. Scale bars: 30  $\mu\text{m}$ .

consistent with the membrane nanopore formation process predicted by our simulations (see Figure 4l).

In addition to SEM, confocal laser scanning microscopy (CLSM) analysis can provide *in vitro* evidence for the pore-forming phenomenon. The interplay between the polypeptide aggregates and the cell membrane was examined. Cell nuclei were stained with 4',6-diamidino-2-phenylindole (DAPI, blue fluorescence), while the cell cytoskeleton was stained with phalloidin (red fluorescence). The green fluorescence represents FITC-labeled polypeptide aggregates. As shown in Figure 5a–d, in comparison with the control group incubated without aggregates, green fluorescence could be observed around the membrane surface. The sphere, toroid-1, toroid-2, and toroid-3 had different uptake efficiencies; that is, these types of aggregates exhibited different fluorescence intensities. Figure 5e shows a quantitative characterization of the internalization process. Clearly, the polypeptide aggregates rapidly entered cells during the first 4 h, and then the rate gradually slowed down. Note that spheres exhibited the most efficient cellular uptake, followed by toroid-1, toroid-2, and toroid-3, which is consistent with simulation results (see Section 1.6 of the Supporting Information). This result shows that toroid-3 is difficult to take up under the present conditions and that the polypeptide toroids with small  $\rho$  values mainly

accumulate around the membrane surface and exhibit pore-forming behavior.

Additionally, the specific interplay between toroid-3 and the membrane is illustrated in Figure 5f,g. The green fluorescence (toroid-3) and red fluorescence (cell cytoskeleton) overlap, which confirms that toroid-3 inserts into the cell membranes. A CLSM 3D overlay image of cells upon incubation with toroid-3 for 6 h is shown in Figure 5h. As seen in the figure, the toroids were located around the membrane surface. By a combination of the CLSM images in Figure 5 and SEM observations in Figure 4, the toroid-induced membrane nanopores are verified. In addition to SMMC-7721 cells, the pore-forming behaviors of the toroids were also observed for HeLa cells, which indicates the universality of the toroid-induced membrane nanopores (see Section 2.6 of the Supporting Information).

From these experiments and simulation predictions, we learned that all the particles used in this work, i.e., toroid-1, toroid-2, toroid-3, and spheres, can interact with the cellular membrane. However, due to the structural characteristics, the uptake behaviors of these particles exhibit differences. Toroid-3 with a large inner cavity stably remains on the cellular membrane, leaving membrane nanopores, while toroid-1, toroid-2, and spheres can be completely endocytosed into the cell and no cellular membrane nanopores can be induced.



In view of the fact that the formation of membrane nanopores by the toroids-3 has been confirmed by SEM and cryo-SEM observations, the formation of membrane nanopores may damage cells due to cytosol leakage,<sup>48</sup> affecting cell activity. Thus, cytotoxicity tests for PBLG spheres, toroid-1, toroid-2, and toroid-3 were performed to support the proposed mechanism and examine the effect of the pore-forming behavior on cell viability (Figure 5i). Since spheres, toroid-1, and toroid-2 cannot induce cellular nanopores, they were expected to exhibit negligible effects on cell viability, which was verified by cytotoxicity studies. As shown in Figure 5i, spheres, toroid-1, and toroid-2 exhibited negligible effects on cell viability at concentrations between 0.1 and 1 g/L. Toroid-3 is able to induce cell nanopores, and it was found that its cytotoxicity depended on the concentration. At 0.1 g/L, toroid-3 exerted slight toxicity on cells. Note that this concentration was slightly higher than that applied in the pore-forming studies (0.09 g/L). Therefore, at a concentration of 0.1 g/L, toroid-3 readily induced cellular nanopores but exerted a minor effect on the viability of the cells. Increasing the concentration decreased cell viability. For the system incubated with toroid-3 at a higher concentration of 1.0 g/L, a 17% decrease in cell viability was observed. The increased cytotoxicity of toroid-3 to cells was presumably related to the formation of excessive nanopores, rendering it difficult for the cells to maintain normal activity. The above studies further support the existence of toroid-induced nanopores, and the viability of cells with nanopores could be maintained at appropriate toroid concentrations.

In this work, we found a cellular pore-forming phenomenon induced by the insertion of nanotoroids in the membrane. In the pathway, membrane lipids wrap through the cavity of the nanotoroid and merge with the lipids outside the nanotoroid, leaving a stable nanopore on the cell. Such a nanotoroid-induced pore-forming pathway is different from that of PFPs, in which the PFPs usually embed in the membrane and assemble into nanopores. This work expands the research scope of cellular uptake and deepens the understanding of nanoparticle–cellular membrane interaction mechanisms. The information gained could promote advances not only in pore-forming technology but also in related nanomedicines and diagnostics.

## CONCLUSION

In summary, we discovered an insertion and pore-forming pathway of nanotoroids on the cellular membrane. CGMD simulations showed that membrane lipids could wrap through the inner cavity of the nanotoroid, and the nanotoroid would stay inside the membrane, creating a nanopore. The pore-forming ability of the nanotoroid can be regulated by both the geometric parameters of the nanotoroid and the membrane–nanotoroid interaction. Under moderate nanotoroid–membrane interactions, a nanotoroid with a relatively large cavity can exhibit pore-forming behavior. The simulation predictions were well confirmed by *in vitro* experimental studies on a system containing polypeptide nanotoroids and living cells. This study revealed a novel pore-forming phenomenon with a unique mechanism, which can assist in the design of advanced pore-forming materials and the development of nanopore technology.

## ASSOCIATED CONTENT

### Supporting Information

The Supporting Information is available free of charge at <https://pubs.acs.org/doi/10.1021/acs.nanolett.1c01331>.

Details regarding the simulation model and method, effects of binding strength, aspect ratio, and ligand distribution, energy calculation, experimental materials and reagents, preparation and characterization of polymers and polypeptide aggregates, and experimental data (PDF)

Movie of the pore-forming behavior (AVI)

Movie of the pore-forming behavior (AVI)

## AUTHOR INFORMATION

### Corresponding Authors

**Jiaping Lin** – Shanghai Key Laboratory of Advanced Polymeric Materials, Key Laboratory for Ultrafine Materials of Ministry of Education, Frontiers Science Center for Materiobiology and Dynamic Chemistry, School of Materials Science and Engineering, East China University of Science and Technology, Shanghai 200237, People's Republic of China; [orcid.org/0000-0001-9633-4483](https://orcid.org/0000-0001-9633-4483); Email: [jlin@ecust.edu.cn](mailto:jlin@ecust.edu.cn)

**Chunhua Cai** – Shanghai Key Laboratory of Advanced Polymeric Materials, Key Laboratory for Ultrafine Materials of Ministry of Education, Frontiers Science Center for Materiobiology and Dynamic Chemistry, School of Materials Science and Engineering, East China University of Science and Technology, Shanghai 200237, People's Republic of China; [orcid.org/0000-0001-9008-6327](https://orcid.org/0000-0001-9008-6327); Email: [caichunhua@ecust.edu.cn](mailto:caichunhua@ecust.edu.cn)

### Authors

**Fangsheng Wu** – Shanghai Key Laboratory of Advanced Polymeric Materials, Key Laboratory for Ultrafine Materials of Ministry of Education, Frontiers Science Center for Materiobiology and Dynamic Chemistry, School of Materials Science and Engineering, East China University of Science and Technology, Shanghai 200237, People's Republic of China

**Xiao Jin** – Shanghai Key Laboratory of Advanced Polymeric Materials, Key Laboratory for Ultrafine Materials of Ministry of Education, Frontiers Science Center for Materiobiology and Dynamic Chemistry, School of Materials Science and Engineering, East China University of Science and Technology, Shanghai 200237, People's Republic of China

**Zhou Guan** – Shanghai Key Laboratory of Advanced Polymeric Materials, Key Laboratory for Ultrafine Materials of Ministry of Education, Frontiers Science Center for Materiobiology and Dynamic Chemistry, School of Materials Science and Engineering, East China University of Science and Technology, Shanghai 200237, People's Republic of China

**Liquan Wang** – Shanghai Key Laboratory of Advanced Polymeric Materials, Key Laboratory for Ultrafine Materials of Ministry of Education, Frontiers Science Center for Materiobiology and Dynamic Chemistry, School of Materials Science and Engineering, East China University of Science and Technology, Shanghai 200237, People's Republic of China; [orcid.org/0000-0002-5141-8584](https://orcid.org/0000-0002-5141-8584)

**Yongsheng Li** – Shanghai Key Laboratory of Advanced Polymeric Materials, Key Laboratory for Ultrafine Materials

of Ministry of Education, Frontiers Science Center for Materiobiology and Dynamic Chemistry, School of Materials Science and Engineering, East China University of Science and Technology, Shanghai 200237, People's Republic of China; [orcid.org/0000-0001-5621-9528](https://orcid.org/0000-0001-5621-9528)

**Shaoliang Lin** – Shanghai Key Laboratory of Advanced Polymeric Materials, Key Laboratory for Ultrafine Materials of Ministry of Education, Frontiers Science Center for Materiobiology and Dynamic Chemistry, School of Materials Science and Engineering, East China University of Science and Technology, Shanghai 200237, People's Republic of China; [orcid.org/0000-0003-3374-9934](https://orcid.org/0000-0003-3374-9934)

**Pengfei Xu** – Shanghai Key Laboratory of Advanced Polymeric Materials, Key Laboratory for Ultrafine Materials of Ministry of Education, Frontiers Science Center for Materiobiology and Dynamic Chemistry, School of Materials Science and Engineering, East China University of Science and Technology, Shanghai 200237, People's Republic of China

**Liang Gao** – Shanghai Key Laboratory of Advanced Polymeric Materials, Key Laboratory for Ultrafine Materials of Ministry of Education, Frontiers Science Center for Materiobiology and Dynamic Chemistry, School of Materials Science and Engineering, East China University of Science and Technology, Shanghai 200237, People's Republic of China; [orcid.org/0000-0001-6852-8301](https://orcid.org/0000-0001-6852-8301)

Complete contact information is available at:  
<https://pubs.acs.org/10.1021/acs.nanolett.1c01331>

#### Author Contributions

†F.W. and X.J. contributed equally.

#### Notes

The authors declare no competing financial interest.

#### ACKNOWLEDGMENTS

This work was supported by the National Natural Science Foundation of China (51621002, 51833003, 52073095, and 21975073). Support from the Project of Shanghai Municipality (20ZR1471300) is also appreciated.

#### REFERENCES

- (1) Conner, S. D.; Schmid, S. L. Regulated portals of entry into the cell. *Nature* **2003**, *422*, 37–44.
- (2) Jiang, W.; Kim, B. Y.; Rutka, J. T.; Chan, W. C. Nanoparticle-mediated cellular response is size-dependent. *Nat. Nanotechnol.* **2008**, *3*, 145–150.
- (3) Sahay, G.; Alakhova, D. Y.; Kabanov, A. V. Endocytosis of nanomedicines. *J. Controlled Release* **2010**, *145*, 182–195.
- (4) Canton, I.; Battaglia, G. Endocytosis at the nanoscale. *Chem. Soc. Rev.* **2012**, *41*, 2718–2739.
- (5) Stewart, M. P.; Langer, R.; Jensen, K. F. Intracellular delivery by membrane disruption: mechanisms, strategies, and concepts. *Chem. Rev.* **2018**, *118*, 7409–7531.
- (6) Doyle, D. A.; Cabral, J. M.; Pfuetzner, R. A.; Kuo, A.; Gulbis, J. M.; Cohen, S. L.; Chait, B. T.; Mackinnon, B. The structure of the potassium channel: molecular basis of K<sup>+</sup> conduction and selectivity. *Science* **1998**, *280*, 69–77.
- (7) Howorka, S. Building membrane nanopores. *Nat. Nanotechnol.* **2017**, *12*, 619–630.
- (8) Valev, I.; Bhakdi, S. C.; Hofmann, F.; Djonder, N.; Valeva, A.; Aktories, K.; Bhakdi, S. Delivery of proteins into living cells by reversible membrane permeabilization with streptolysin-O. *Proc. Natl. Acad. Sci. U. S. A.* **2001**, *98*, 3185–3190.

(9) Stewart, M. P.; Sharei, A.; Ding, X.; Sahay, G.; Langer, R.; Jensen, K. F. In vitro and ex vivo strategies for intracellular delivery. *Nature* **2016**, *538*, 183–192.

(10) Gilbert, R. J.; Dalla Serra, M.; Froelich, C. J.; Wallace, M. I.; Anderluh, G. Membrane pore formation at protein-lipid interfaces. *Trends Biochem. Sci.* **2014**, *39*, 510–516.

(11) van Pee, K.; Mulvihill, E.; Müller, D. J.; Yildiz, Ö. Unraveling the pore-forming steps of pneumolysin from streptococcus pneumoniae. *Nano Lett.* **2016**, *16*, 7915–7924.

(12) Mulvihill, E.; van Pee, K.; Mari, S. A.; Müller, D. J.; Yildiz, Ö. Directly observing the lipid-dependent self-assembly and pore-forming mechanism of the cytolytic toxin Listeriolysin O. *Nano Lett.* **2015**, *15*, 6965–6973.

(13) Dal Peraro, M.; van der Goot, F. G. Pore-forming toxins: ancient, but never really out of fashion. *Nat. Rev. Microbiol.* **2016**, *14*, 77–92.

(14) Gilbert, R. J. Protein-lipid interactions and non-lamellar lipidic structures in membrane pore formation and membrane fusion. *Biochim. Biophys. Acta, Biomembr.* **2016**, *1858*, 487–499.

(15) Gilbert, R. J. Electron microscopy as a critical tool in the determination of pore forming mechanisms in proteins. *Methods Enzymol.* **2021**, *649*, 71–102.

(16) Berman, H. M.; Westbrook, J.; Feng, Z.; Gilliland, G.; Bhat, T. N.; Weissig, H.; Shindyalov, I. N.; Bourne, P. E. The Protein Data Bank. *Nucleic Acids Res.* **2000**, *28*, 235–242.

(17) Lichtenberg, D.; Ahyayauch, H.; Goni, F. M. The mechanism of detergent solubilization of lipid bilayers. *Biophys. J.* **2013**, *105*, 289–299.

(18) Geng, J.; Kim, K.; Zhang, J.; Escalada, A.; Tunuguntla, R.; Comolli, L. R.; Allen, F. I.; Shnyrova, A. V.; Cho, K. R.; Munoz, D.; Wang, Y. M.; Grigoropoulos, C. P.; Ajo-Franklin, C. M.; Frolov, V. A.; Noy, A. Stochastic transport through carbon nanotubes in lipid bilayers and live cell membranes. *Nature* **2014**, *514*, 612–615.

(19) Lopez, C. F.; Nielsen, S. O.; Moore, P. B.; Klein, M. L. Understanding nature's design for a nanosyringe. *Proc. Natl. Acad. Sci. U. S. A.* **2004**, *101*, 4431–4434.

(20) Ding, X.; Stewart, M.; Sharei, A.; Weaver, J. C.; Langer, R. S.; Jensen, K. F. High-throughput nuclear delivery and rapid expression of DNA via mechanical and electrical cell-membrane disruption. *Nat. Biomed. Eng.* **2017**, *1*, 1–7.

(21) García-López, V.; Chen, F.; Nilewski, L. G.; Duret, G.; Aliyan, A.; Kolomeisky, A. B.; Robinson, J. T.; Wang, G.; Pal, R.; Tour, J. M. Molecular machines open cell membranes. *Nature* **2017**, *548*, 567–572.

(22) Shalek, A. K.; Robinson, J. T.; Karp, E. S.; Lee, J. S.; Ahn, D. R.; Yoon, M. H.; Sutton, A.; Jorgolli, M.; Gertner, R. S.; Gujral, T. S.; MacBeath, G.; Yang, E. G.; Park, H. Vertical silicon nanowires as a universal platform for delivering biomolecules into living cells. *Proc. Natl. Acad. Sci. U. S. A.* **2010**, *107*, 1870–1875.

(23) Huang, C.; Zhang, Y.; Yuan, H.; Gao, H.; Zhang, S. Role of nanoparticle geometry in endocytosis: laying down to stand up. *Nano Lett.* **2013**, *13*, 4546–4550.

(24) Xu, Y.; Luo, Z.; Li, S.; Li, W.; Zhang, X.; Zuo, Y. Y.; Huang, F.; Yue, T. Perturbation of the pulmonary surfactant monolayer by single-walled carbon nanotubes: a molecular dynamics study. *Nanoscale* **2017**, *9*, 10193–10204.

(25) Wang, X.; Wang, X.; Bai, X.; Yan, L.; Liu, T.; Wang, M.; Song, Y.; Hu, G.; Gu, Z.; Miao, Q.; Chen, C. Nanoparticle ligand exchange and its effects at the nanoparticle-cell membrane interface. *Nano Lett.* **2019**, *19*, 8–18.

(26) Yang, K.; Ma, Y. Q. Computer simulation of the translocation of nanoparticles with different shapes across a lipid bilayer. *Nat. Nanotechnol.* **2010**, *5*, 579–583.

(27) Chen, P.; Yue, H.; Zhai, X.; Huang, Z.; Ma, G.-H.; Wei, W.; Yan, L.-T. Transport of a graphene nanosheet sandwiched inside cell membranes. *Sci. Adv.* **2019**, *5*, No. eaaw3192.

(28) Garcia-Fandino, R.; Pineiro, A.; Trick, J. L.; Sansom, M. S. Lipid bilayer membrane perturbation by embedded nanopores: a simulation study. *ACS Nano* **2016**, *10*, 3693–3701.



- (29) Li, X.; Gu, M.; Zhang, L.; Lin, J. Computational investigation on the superstructures of micelles from amphiphilic DNA block copolymers. *Acta Polym. Sin.* **2020**, *51*, 1257–1266.
- (30) Shi, X.; von dem Bussche, A.; Hurt, R. H.; Kane, A. B.; Gao, H. Cell entry of one-dimensional nanomaterials occurs by tip recognition and rotation. *Nat. Nanotechnol.* **2011**, *6*, 714–719.
- (31) Xue, J.; Guan, Z.; Zhu, X.; Lin, J.; Cai, C.; Jin, X.; Li, Y.; Ye, Z.; Zhang, W.; Jiang, X. Cellular internalization of polypeptide-based nanoparticles: effects of size, shape and surface morphology. *Biomater. Sci.* **2018**, *6*, 3251–3261.
- (32) Cooke, I. R.; Deserno, M. Solvent-free model for self-assembling fluid bilayer membranes: stabilization of the fluid phase based on broad attractive tail potentials. *J. Chem. Phys.* **2005**, *123*, 224710.
- (33) Guan, Z.; Wang, L.; Lin, J. Interaction pathways between plasma membrane and block copolymer micelles. *Biomacromolecules* **2017**, *18*, 797–807.
- (34) Vácha, R.; Martínez-Veracochea, F. J.; Frenkel, D. Receptor-mediated endocytosis of nanoparticles of various shapes. *Nano Lett.* **2011**, *11*, 5391–5395.
- (35) Ting, C. L.; Appelo, D.; Wang, Z. G. Minimum energy path to membrane pore formation and rupture. *Phys. Rev. Lett.* **2011**, *106*, 168101.
- (36) Shen, Z.; Ye, H.; Yi, X.; Li, Y. Membrane wrapping efficiency of elastic nanoparticles during endocytosis: size and shape matter. *ACS Nano* **2019**, *13*, 215–228.
- (37) Zhang, S.; Li, J.; Lykotrafitis, G.; Bao, G.; Suresh, S. Size-dependent endocytosis of nanoparticles. *Adv. Mater.* **2009**, *21*, 419–424.
- (38) Helfrich, W. Elastic properties of lipid bilayers: theory and possible experiments. *Z. Naturforsch., C: J. Biosci.* **1973**, *28*, 693–703.
- (39) Yang, C.; Gao, L.; Lin, J.; Wang, L.; Cai, C.; Wei, Y.; Li, Z. Toroid formation through a supramolecular “cyclization reaction” of rodlike micelles. *Angew. Chem., Int. Ed.* **2017**, *56*, 5546–5550.
- (40) Xu, P.; Gao, L.; Cai, C.; Lin, J.; Wang, L.; Tian, X. Helical toroids self-assembled from a binary system of polypeptide homopolymer and its block copolymer. *Angew. Chem., Int. Ed.* **2020**, *59*, 14281–14285.
- (41) Pochan, D. J.; Chen, Z.; Cui, H.; Hales, K.; Qi, K.; Wooley, K. L. Toroidal triblock copolymer assemblies. *Science* **2004**, *306*, 94–97.
- (42) Cai, C.; Lin, J.; Lu, Y.; Zhang, Q.; Wang, L. Polypeptide self-assemblies: nanostructures and bioapplications. *Chem. Soc. Rev.* **2016**, *45*, 5985–6012.
- (43) Nel, A. E.; Mädler, L.; Velegol, D.; Xia, T.; Hoek, E. M.; Somasundaran, P.; Klaessig, F.; Castranova, V.; Thompson, M. Understanding biophysicochemical interactions at the nano-bio interface. *Nat. Mater.* **2009**, *8*, 543–557.
- (44) Krumm, B. E.; Grishammer, R. Peptide ligand recognition by G protein-coupled receptors. *Front. Pharmacol.* **2015**, *6*, 48.
- (45) Burns, J. R.; Al-Juffali, N.; Janes, S. M.; Howorka, S. Membrane-spanning DNA nanopores with cytotoxic effect. *Angew. Chem., Int. Ed.* **2014**, *53*, 12466–12470.
- (46) Xue, J.; Guan, Z.; Lin, J.; Cai, C.; Zhang, W.; Jiang, X. Cellular internalization of rod-like nanoparticles with various surface patterns: novel entry pathway and controllable uptake capacity. *Small* **2017**, *13*, 1604214.
- (47) van Pee, K.; Neuhaus, A.; D’Imprima, E.; Mills, D. J.; Kühlbrandt, W.; Yildiz, Ö. CryoEM structures of membrane pore and prepore complex reveal cytolytic mechanism of Pneumolysin. *eLife* **2017**, *6*, No. e23644.
- (48) Tang, S. K. Y.; Marshall, W. F. Self-repairing cells: how single cells heal membrane ruptures and restore lost structures. *Science* **2017**, *356*, 1022–1025.